

# Ab Initio Determination of Reversible Potentials and Activation Energies for Outer-Sphere Oxygen Reduction to Water and the Reverse Oxidation Reaction

Alfred B. Anderson\* and Titus V. Albu

Contribution from the Department of Chemistry, Case Western Reserve University, Cleveland, Ohio 44106-7078

Received August 2, 1999. Revised Manuscript Received October 21, 1999

**Abstract:** The outer-sphere reduction of oxygen to water according to  $\text{O}_2(\text{g}) + 4\text{H}^+(\text{aq}) + 4\text{e}^- \rightarrow 2\text{H}_2\text{O}(\text{l})$  (1) and its reverse reaction are analyzed using self-consistent ab initio MP2/6-31G\*\* calculations over the electrode potential range of  $U = 0-2$  V ( $\text{H}^+/\text{H}_2$ ). Activation energies are calculated for each of the four one-electron steps:  $\text{O}_2 + \text{H}^+ + \text{e}^-(U) \rightarrow \text{HOO}^\bullet$  (2);  $\text{HOO}^\bullet + \text{H}^+ + \text{e}^-(U) \rightarrow \text{H}_2\text{O}_2$  (3);  $\text{H}_2\text{O}_2 + \text{H}^+ + \text{e}^-(U) \rightarrow \text{HO}^\bullet + \text{H}_2\text{O}$  (4); and  $\text{HO}^\bullet + \text{H}^+ + \text{e}^-(U) \rightarrow \text{H}_2\text{O}$  (5). In the calculational model  $\text{H}^+$  is a hydronium ion with two water molecules hydrogen bonded to it. The electrode potential is given by  $U/\text{V} = \varphi/\text{eV} - \varphi_{\text{H}^+/\text{H}_2}/\text{eV}$  (6) where  $\varphi$  and  $\varphi_{\text{H}^+/\text{H}_2}$  are the thermodynamic work functions of the electrode surface and of the standard hydrogen electrode surface, respectively. Electron transfer is assumed to occur when the electron affinity, EA, of the reaction complex equals the ionization potential, IP, of the electrode and there is an equilibrium so that  $\varphi = \text{IP} = \text{EA}$ . The electron transfers to an  $\text{RO}^\bullet \cdots \text{H}^+ \cdots \text{OH}_2(\text{OH}_2)$  orbital that is  $\text{H}^+ \cdots \text{OH}_2$  antibonding and  $\text{RO}^\bullet \cdots \text{H}^+$  bonding and this orbital is greatly stabilized by the electric field due to the positive charge. Over the potential range considered, activation energies for the reduction reactions decrease in the sequence (4) > (2) > (3) > (5). For the reverse reactions the activation energies decrease according to (5) > (4)  $\approx$  (3) > (2). It is found that calculated reversible potentials,  $U^\circ$ , as determined simply from reaction energies for reactions 1, 4, 5, 2 + 3 and reactions 4 + 5 differ from the measured values by a constant.

## A. Introduction

**1. Background on Electron-Transfer Theory.** Electrochemical redox reactions involve electron transfer between the electrode and the reaction center. Gurney introduced in 1931 a quantum mechanical model for the electrode current generated by outer-sphere redox reactions.<sup>1</sup> The important properties of the electrode were represented by the surface electron distribution function,  $n(E,U)$ , where  $E$  is the energy of an electron and  $U$  is the electrode potential, which is equal to a constant minus the Fermi energy,  $E_F$ . This was multiplied by the ion distribution function,  $N(E,x)$ , where  $E$  is the energy of an ion state and  $x$  is the distance of the ion from the electrode surface. The electron was assumed to transfer between the electrode surface and the ion in solution by radiationless tunneling, so an electron tunneling factor,  $P_T(E,x)$ , was introduced. The predicted electrode current was then proportional to this three-term product integrated over  $E$  and  $x$ . Applications of the full formalism of Gurney are rare and have required model assumptions, as are seen in the work of Bockris and Abdu, who have recently treated the first step in oxygen reduction.<sup>2</sup>

From the phenomenological viewpoint, the linear regions of Tafel plots of the log of electrode current as a function of overpotential are explained using absolute rate theory. The

dependence of the activation Gibbs energy,  $\Delta G^*$ , on overpotential is assumed to be linear. Thus, for oxidation

$$\Delta G_{\text{ox}}^*(\eta) = \Delta G^*(U^\circ) - \alpha F\eta \quad (1)$$

and for reduction

$$\Delta G_{\text{rd}}^*(\eta) = \Delta G^*(U^\circ) + \beta F\eta \quad (2)$$

where  $\eta$  is the overpotential,  $U^\circ$  is the reversible potential,  $F$  is Faraday's constant,  $\alpha$  is the linear constant, and  $\beta$  is  $1 - \alpha$ . The electrode current is then given by the Butler–Volmer equation<sup>3</sup>

$$i = j_0 [e^{\alpha F\eta/RT} - e^{-(1-\alpha)F\eta/RT}] \quad (3)$$

where  $j_0$  is the exchange current, which is the preexponential factor of the absolute rate theory.

In the widely adopted harmonic model, the activation Gibbs energy is assumed to vary with overpotential according to

$$\Delta G_{\text{ox}}^*(\eta) = (\lambda - F\eta)^2/4\lambda \quad (4)$$

(1) Gurney, R. W. *Proc. R. Soc.* **1931**, A 134, 137–154.  
(2) Bockris, J. O'M.; Abdu, R. J. *Electroanal. Chem.* **1998**, 448, 189–204.

(3) For more discussion, see: Miller, R. J. D.; McLendon, G. L.; Nozik, A. J.; Schmickler, W.; Willig, F. *Surface Electron-Transfer Processes*; VCH: New York, 1995; Section 3.2.

for oxidation and

$$\Delta G_{\text{red}}^*(\eta) = (\lambda + F\eta)^2/4\lambda \quad (5)$$

for reduction, where  $\lambda$  is solvent reorganization energy.<sup>4–6</sup> The solvent reorganization energy has been incorporated into quantum mechanical-based electron-transfer equations by Marcus, Gerischer, Levich and Dogonadze, and others.<sup>4,5</sup> These formalisms have been used in thinking about outer-sphere electron transfer reactions where electron tunneling is associated with a sudden change in redox state. For redox centers that are in contact with an electrode surface, the redox reaction may instead proceed smoothly and incrementally as a function of reaction progress. Hush introduced the corresponding adiabatic electron-transfer model and has shown how it can relate to the harmonic model of eqs 4 and 5.<sup>6</sup> The adiabatic concept has been applied by Schmickler and others<sup>7</sup> for inner-Helmholtz-plane surface-activated redox reactions. Modeling simplifications are currently used to make studies of this type computationally feasible. For example, in a recent study by Koper and Voth,<sup>8</sup> Cl<sub>2</sub> reduction was broken into two steps with a different Hamiltonian for each, only the Cl<sub>2</sub> LUMO (lowest unoccupied molecular orbital) was used, electronic interactions with the electrode surface were modeled, Morse potentials were used to obtain the potential energy surface, and the Marcus–Hush model was used for estimating the solvent relaxation energy. Potential dependent activation energies were one of the interesting, though very approximate, products of this work.

**2. An Ab Initio Theory for Outer-Helmholtz-Plane Electron-Transfer Reactions.** This lab has recently undertaken a program of study with the goal of calculating the dependence on electrode potential of activation energies for outer-Helmholtz-plane redox reactions using accurate ab initio quantum mechanics. Activation energy has long been a significant parameter for understanding homogeneous and heterogeneous catalysis. Just as in these areas of catalysis, understanding the structure and electronic factors controlling reaction barriers can become important to electrocatalysis. One of the electronic factors, the electron chemical potential, or potential of the electrode surface, is an adjustable variable in electrochemistry. Two studies of the effects of changing an electrode potential have been completed. The first was a calculation of the potential dependence of the hydrogen evolution reaction over the hydrogen terminated diamond electrode by reduction of the hydronium ion.<sup>9</sup> Oversimplified diamond surface and hydronium ion models were used along with minimal basis set uncorrelated HF/STO-3G wave functions. No double layer effects were included. The electron at various electrode potentials was provided by the noninteracting donor molecule of adjustable ionization potential. Convergence was sometimes incorrect, making it necessary to extrapolate the transition state structure and activation energy. More recently, preliminary results related to the four one-electron O<sub>2</sub> to 2 H<sub>2</sub>O outer-Helmholtz-plane reduction steps based on a solvated hydronium ion model and a more accurate MP2/6-31G\*\* wave function were communicated.<sup>10</sup> To avoid

computational convergence problems, the energy surfaces for the reactant plus electron and for the product were calculated and the transition state was identified as the lowest energy point of intersection of these surfaces. In the present paper the variable electrode potential and reaction center models and the structure and electronic factors operating in the oxygen reduction study are analyzed in detail. The reverse reaction, water oxidation to O<sub>2</sub>, is also discussed.

**3. Background on Electrochemical Oxygen Reduction.** On platinum, which is the best O<sub>2</sub> reducing electrode employed in hydrogen and hydrocarbon fuel cells containing acid electrolytes to date, significant currents (~100 mA per cm<sup>2</sup> of electrode surface) begin to flow at ~300 mV overpotential, that is, at around 0.9 V (SHE)<sup>11</sup> (the reversible potential for O<sub>2</sub> reduction to water is 1.229 V;<sup>12</sup> all potentials given in this paper are referenced to the standard hydrogen electrode). Minimizing the overpotential is sought, and in the case of platinum, the effects of anion adsorption,<sup>13,14</sup> surface structure,<sup>13–15</sup> and alloying with other transition metals<sup>16–18</sup> are being studied. Many of the significant issues are covered in Adzic's recent review of oxygen reduction.<sup>14</sup>

The orientation of O<sub>2</sub> on the electrode surface and its ability to bond to the surface play a role on other electrodes as well, such as gold and silver,<sup>14,19,20</sup> and quantum chemistry has been used to explore these effects on the Ag(100) electrode.<sup>21</sup> Transition metal oxides show promise as oxygen reducing electrocatalysts<sup>22</sup> and quantum chemistry has addressed some of the electronic and mechanistic aspects.<sup>23</sup> Transition metal macrocyclic complexes supported on electrodes are also being studied in this context and a number of mechanistic questions have been raised.<sup>24–27</sup> In a recent study of an Fe/Cu complex a clean four-electron electroreduction of oxygen was observed but at a high overpotential.<sup>28</sup> Pyrolyzed transition metal macrocyclic complexes on graphite electrodes have been found

(11) See, for example: Srinivasan, S.; Parthasarathy, A.; Valev, O. A.; Ferreira, A. C.; Mukerjee, S.; Appelby, A. *J. Proc. Electrochem. Soc.* **1992**, 92–11, 474–493.

(12) Hoare, J. P. In *Standard Potentials in Aqueous Solution*; Bard, A. J., Parsons, R., Jordan, J., Eds.; Marcel Dekker: New York, 1985; *Handbook of Chemistry and Physics*, 67th ed.; Weast, C. R., Ed.; CRC Press: Boca Raton, FL, 1986.

(13) Markovic, N. M.; Adzic, R. R.; Cahan, B. D.; Yeager, E. B. *J. Electroanal. Chem.* **1994**, 337, 249–259.

(14) Adzic, R. In *Electrocatalysis*; Lipkowsky, J., Ross, P. N., Eds.; Wiley: New York, 1998; pp 197–242.

(15) Markovic, N. M.; Gasteiger, H. A.; Ross, P. N., Jr. *J. Phys. Chem.* **1995**, 99, 3411–3415.

(16) Mukerjee, S.; Srinivasan, S.; Soriaga, M. P.; McBreen, J. *J. Phys. Chem.* **1995**, 99, 4577–4589. Mukerjee, S.; Srinivasan, S.; Soriaga, M. P.; McBreen, J. *J. Electrochem. Soc.* **1995**, 142, 1409–1422.

(17) Paffett, M. T.; Berry, J. G.; Gottesfeld, S. *J. Electrochem. Soc.* **1988**, 135, 1431–1436.

(18) Kim, K. T.; Kim, Y. G.; Chung, J. S. *J. Electrochem. Soc.* **1995**, 142, 1531–1538.

(19) Yeager, E. *Electrochim. Acta* **1984**, 29, 1527–1537.

(20) Tarasevich, M.; Sadkowsky, A.; Yeager, E. In *Comprehensive Treatise of Electrochemistry*; Conway, B. E., Bockris, J. O'M., Yeager, E., Khan, S. U. M., White, R. E., Eds.; Plenum: New York, 1983; Vol. 7, p 301.

(21) Mehandru, S. P.; Anderson, A. B. *Surf. Sci.* **1989**, 216, 105–124.

(22) Goodenough, J. B.; Manoharan, R. *Proc. Electrochem. Soc.* **1992**, 92–11, 523–539.

(23) Anderson, A. B. *Proc. Electrochem. Soc.* **1992**, 92–11, 434–439.

(24) Vasudevan, P.; Santosh; Mann, N.; Tyagi, S. *Transition Met. Chem.* **1990**, 15, 81–90.

(25) Coutanceau, C.; Crougneau, P.; Léger, J. M.; Lamy, C. *J. Electroanal. Chem.* **1994**, 379, 389–397.

(26) Shi, C.; Anson, F. C. *Inorg. Chem.* **1996**, 35, 7928–7931.

(27) Collman, J. P.; Ennis, M. S.; Offord, D. A.; Chug, L. L.; Griffin, J. H. *Inorg. Chem.* **1996**, 35, 1751–1752.

(28) Collman, J. P.; Rapta, M.; Broring, M.; Raptova, L.; Schwenninger, R.; Boitrel, B.; Fu, L.; L'Her, M. *J. Am. Chem. Soc.* **1999**, 121, 1387–1388 and available Supporting Information.

(4) Marcus, R. A.; Sutin, N. *Biochim. Biophys. Acta* **1985**, 811, 265–323.

(5) Reference 3, Section 3.3.

(6) Hush, N. S. *J. Electroanal. Chem.* **1999**, 460, 5–29.

(7) Koper, T. M.; Schmickler, W. In *Electrocatalysis*; Lipkowsky, J., Ross, P. N., Eds.; Wiley: New York, 1998; pp 291–322.

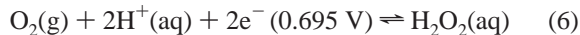
(8) Koper, M. T. M.; Voth, G. A. *J. Chem. Phys.* **1998**, 109, 1991–2001.

(9) Anderson, A. B.; Kang, D. B. *J. Phys. Chem.* **1998**, A102, 5993–5996.

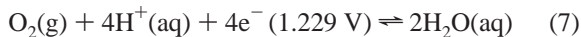
(10) Anderson, A. B.; Albu, T. V. *Electrochem. Comm.* **1999**, 1, 203–206.

active, and have raised further mechanistic questions concerning the role of nitrogen<sup>29</sup> and the metal<sup>30</sup> in activating O<sub>2</sub> reduction.

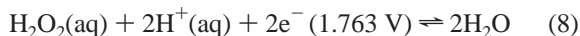
In some cases oxygen reduction cathodes generate hydrogen peroxide, which has a 0.695 V reversible potential:<sup>12</sup>



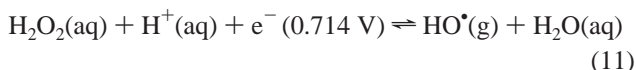
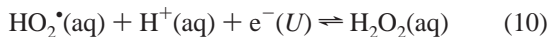
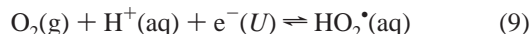
This should not be an issue during efficient low-overpotential four-electron reduction:



Some electrode surfaces are capable of only two-electron reduction to hydrogen peroxide<sup>14,15,19–21,24</sup> and others perform a four-electron reduction to water indirectly in two-electron steps,<sup>16,25,26</sup> namely, reaction 6 and



the latter having a very high reversible potential so that the four-electron pathway where H<sub>2</sub>O<sub>2</sub>(aq) is an intermediate wastes Gibbs energy. However, if H<sub>2</sub>O<sub>2</sub>(ads) is an intermediate in the catalyzed direct four-electron reduction process, it must be stabilized by bonding to a catalytic site. The nature of catalytic factors that lower the activation energies for the four proton and electron transfers are of great interest. It is noted that reversible potentials for the intermediate noncatalyzed solution-phase steps in oxygen reduction to water are well-known only for the last two steps:<sup>12</sup>



Given here is a first stage quantum chemical analysis of the oxygen reduction process. Potential-dependent activation energies are calculated for the four outer-Helmholtz-plane steps in the four-electron reduction of oxygen to water, reactions 9–12. The results will be benchmarks for subsequent studies of oxygen reduction catalysis. As an ancillary effort, also presented are the calculated potential dependent activation energies for the four outer-Helmholtz-plane steps of water oxidation to oxygen based on the fact that the transition states are the same as for reduction.

## B. Theoretical Method

**1. Model for Electrode Potentials.** The chemical potential,  $\mu$ , of electrons at the electrode surface is the Fermi energy,  $E_F$ , which is also equal to the negative of the thermodynamic work function of the surface,  $\varphi$ , and is a function of the surface ionization potential, IP, and electron affinity, EA (all with eV units). At 0 K this function is

$$\mu = E_F = -\varphi = -(\text{IP} + \text{EA})/2 \quad (13)$$

and this formula is assumed for this study. On the standard hydrogen electrochemical (SHE) scale the electrode potential  $U$  (V) is given as

(29) Biloul, A.; Gouérec, P.; Savy, M.; Scarbeck, G.; Besse, S.; Riga, J. *J. Appl. Electrochem.* **1996**, *26*, 1139–1146.

(30) Lalonde, G.; Cote, R.; Guay, D.; Dodelet, J. P.; Weng, L. T.; Bertrand, P. *Electrochim. Acta* **1997**, *42*, 1379–1388.

$$U/V = \varphi/\text{eV} - \varphi_{\text{H}^+/\text{H}_2}/\text{eV} \quad (14)$$

where  $\varphi_{\text{H}^+/\text{H}_2}$  is the thermodynamic work function of the standard hydrogen electrode. Experimental estimates of  $\varphi_{\text{H}^+/\text{H}_2}$  yield a range of values and the average value, 4.6 eV,<sup>31</sup> is used in the current work.

Let the electrode, which is a source of electrons for reduction reactions or an electron sink for oxidation reactions, be modeled by a donor entity, D, with a particular ionization potential for reduction reactions or an electron acceptor entity, A, with a particular electron affinity for oxidation reactions. Suppose that D or A is able to exchange an electron with a reaction center but otherwise does not interact with it, as is the case for outer-Helmholtz-plane redox reactions. Consider a reduction reaction and let the donor ionization potential have the value IP\*. As the reaction center, R, that is to undergo reduction changes its structure due to thermal motion, its electron affinity also changes. Let a structure R\* be reached with electron affinity EA\* equal to IP\*. Then an equilibrium between the donor and activated reaction center, R\*, is assumed:



The thermodynamic work function of the equilibrium system D + R\* is, from eq 13, IP\*, and so, from eq 14, the modeled electrode potential is

$$U/V = \text{IP}^*/\text{eV} - 4.6 \quad (16)$$

To study an oxidation reaction an electron acceptor species of adjustable electron affinity, EA, is considered. This could be an ionized donor of the type just mentioned. The process of finding the potential-dependent transition states and activation energies would parallel the reduction process and would focus on finding the lowest energy pathway through an equilibrium of the form



where A is the acceptor species and, on the hydrogen scale, the electrode potential would be

$$U/V = \text{EA}^*/\text{eV} - 4.6 \quad (18)$$

In the case of O<sub>2</sub> reduction and hydrogen evolution as studied previously<sup>9,10</sup> the electron transfers coincided with the reaction transition states because of concomitant bond order changes. In general, electron transfers need not coincide with transition states and could occur before or after the transition state (maximum energy along the reaction path) structures are reached.

It is possible to eliminate the donor or acceptor species from the calculations by making a careful analysis of the intersections of the reactant Born–Oppenheimer potential energy surface with that for the reduced or oxidized product.<sup>9,10</sup> This avoids the calculational problem of the electron not always transferring from a remote donor when it would be more stable to do so. In this study all reported results are from the calculation of two energy surfaces. Further details of the explicit donor approach may be found in the earlier paper on hydrogen reduction from diamond electrodes.<sup>9</sup>

**2. Computational Details.** All activation energies were found by means of charge self-consistent MP2/6-31G\*\* calculations using the Gaussian 94 package of programs.<sup>32</sup> Additional calculations with other wave functions were performed for comparative purposes, as will be discussed below.

(31) Bockris, J. O'M.; Khan, S. U. M. *Surface Electrochemistry*; Plenum Press: New York, 1993; p 493.

(32) *Gaussian 94* (Revision C.3), Frisch, M. J.; Trucks, G. W.; Schlegel, H. B.; Gill, P. M. W.; Johnson, B. G.; Robb, M. A.; Cheeseman, J. R.; Keith, T. A.; Petersson, G. A.; Montgomery, J. A.; Raghavachari, K.; Al-Laham, M. A.; Zakrzewski, V. G.; Ortiz, J. V.; Foresman, J. B.; Cioslowski, J.; Stefanov, B. B.; Nanayakkara, A.; Challacombe, M.; Peng, C. Y.; Ayala, P. Y.; Chen, W.; Wong, M. W.; Andres, J. L.; Replogle, E. S.; Gomperts, R.; Martin, R. L.; Fox, D. J.; Binkley, J. S.; Defrees, D. J.; Baker, J.; Stewart, J. P.; Head-Gordon, M.; Gonzalez, C.; Pople, J. A., Gaussian, Inc.: Pittsburgh, PA, 1995.

**Table 1.** Calculated Equilibrium Internuclear Distances,  $R_e$  (Å), and Bond Angles,  $\theta_e$  (deg), for the Hydronium Ion,  $H_3O^+$ , with 0–3  $H_2O$  Molecules Hydrogen Bonded to It, along with Calculated Proton Stabilization Energies<sup>a</sup>

method	molecule	$R_e$ (O–H <sub>i</sub> )	$R_e$ (O–H <sub>s</sub> )	$\theta_e$ (H <sub>s</sub> OH <sub>i</sub> )	$\theta_e$ (H <sub>s</sub> OH <sub>s</sub> )	$\theta_e$ (H <sub>i</sub> OH <sub>i</sub> )	$R_e$ (H <sub>s</sub> ··OH <sub>2</sub> )	$\theta_e$ (OH <sub>s</sub> O)	$R_e$ (O–H <sub>a</sub> )	$R_e$ (O–H <sub>b</sub> )	$\theta_e$ (H <sub>s</sub> OH <sub>a</sub> )	$\theta_e$ (H <sub>s</sub> OH <sub>b</sub> )	$\theta_e$ (H <sub>a</sub> OH <sub>b</sub> )	proton stabilization energy (eV)
HF	$H_3O^+$	0.961				114.7								7.80
	$H_3O^+(H_2O)$	0.952	1.081	118.4		112.7	1.314	180.0	0.949	0.948	123.8	126.0	110.2	9.27
	$H_3O^+(H_2O)_2$	0.950	1.002	114.6	117.8		1.514	180.0	0.947	0.946	123.9	127.8	108.3	10.35
	$H_3O^+(H_2O)_3$		0.982		115.5		1.607	180.0	0.946	0.945	123.8	128.4	107.8	11.25
MP2	$H_3O^+$	0.979				112.5								7.79
	$H_3O^+(H_2O)$	0.969	1.152	117.6		110.2	1.231	180.0	0.966	0.965	123.5	125.4	111.1	9.47
	$H_3O^+(H_2O)_2$	0.967	1.035	112.8	116.8		1.444	180.0	0.964	0.963	123.9	128.2	107.9	10.64
	$H_3O^+(H_2O)_3$		1.008		113.9		1.540	180.0	0.963	0.963	123.8	129.2	107.0	11.61
MP4	$H_3O^+$	0.978				112.4								7.83
	$H_3O^+(H_2O)$	0.968	1.191	118.5		109.6	1.194	180.0	0.968	0.967	118.0	119.4	109.6	9.49
	$H_3O^+(H_2O)_2$	0.966	1.031	112.7	116.3		1.454	180.0	0.963	0.963	124.1	128.2	107.7	10.63
	$H_3O^+(H_2O)_3$		1.005		113.6		1.549	180.0	0.963	0.962	123.8	129.2	107.7	11.59
MP2	$H_3O^+(H_2O)_2$	0.966	1.040	112.9	115.6		1.438	175.3	0.965	0.964	121.2	125.9	107.4	10.65

<sup>a</sup> Structure parameters are defined in Figure 2. The various levels of calculations are all with a 6-31G\*\* basis set. The 180.0° value for OH<sub>s</sub>O is assumed. The 175.3° value for the last entry is optimized, and this is the structure used for the reaction studies.

It is well-known that for the calculation of accurate electron affinity, diffuse functions must be included in the basis set. Thus, for example, MP2/6-31G\*\* calculations predict an electron affinity of –0.16 eV for HO\*(g). However, the MP2/6-311 + G(2df,p) approach yields 1.81 eV,<sup>33</sup> closer to the 1.83 eV<sup>34</sup> experimental value, due to the presence of additional diffuse atomic orbital functions. The electron affinities of the reactants at the transition states in this work are large, 4.6 to 6.6 eV for the  $U = 0$  to 2 V electrode potential range. Molecules of high electron affinity are expected to be less sensitive to the presence of diffuse functions, for example, Li<sub>2</sub><sup>+</sup> has a measured EA of 5.11 eV<sup>35</sup> while MP2/6-31G\*\* and MP2/6-311 + G(2df,p) results are 4.70 and 4.80 eV, respectively. Consequently the smaller and more computationally tractable 6-31G\*\* basis set is used for obtaining the electron-transfer activation energies in this paper. This basis set yields, as shown below, bond strengths of suitable accuracy.

## C. Results and Discussion

**1. Reversible Potentials for Reactions 6–8, 11, and 12. a. Proton Solvation.** The solvated proton participates in each reaction, so models were explored for it at the HF, MP2, and MP4 levels based on the 6-31G\*\* basis set. As shown in Table 1, adding one, two, and three water molecules to  $H_3O^+$  brings the proton solvation energy at the correlation-corrected MP2 and MP4 levels to 0.3 eV above the experimental value of 11.305 eV.<sup>36</sup> Table 1 also gives the calculated structure parameters for these systems. There will be some reorientation of the hydrogen-bonded water network around  $H_3O^+$ , and this is not calculated in the present model. However, the magnitude of the reorientation energy can be estimated as follows. When a proton enters liquid water, it disrupts the hydrogen-bonded network by occupying a lone-pair of one  $H_2O$  molecule. It thereby essentially annihilates one of the hydrogen bonds in the water network. Given the standard 0.46 eV vaporization enthalpy of  $H_2O(l)$ ,<sup>12</sup> and the presence of two strong hydrogen bonds per  $H_2O$  molecule, the loss of one hydrogen bond means that the calculated proton stabilization will be reduced by about 0.23 eV, putting the values in Table 1 closer to experiment. A

(33) Hrusak, J.; Friedrichs, H.; Schwartz, H.; Razafinjanahary, H.; Chermette, H. *J. Phys. Chem.* **1996**, *100*, 100–110.

(34) Huber, K. P.; Herzberg, G. *Molecular Spectra and Molecular Structure, Vol. IV. Constants of Diatomic Molecules*; van Nostrand Reinhold: New York, 1979; p 516.

(35) McGeoch, M. W.; Shlier, R. E. *Chem. Phys. Lett.* **1983**, *99*, 347–352.

(36) See Footnote 31, p 492.

(37) Based on –21 J deg mol<sup>–1</sup> estimated entropy of proton solvation as given by: Atkins, P. *Physical Chemistry*, 6th ed.; Freeman: New York, 1997; p 247.

**Table 2.** Calculated Bond Strengths (eV) Using Various Methods, but Not Including Zero-Point Vibrational Energies, Compared with Measured Values

reaction	method					(exptl) <sup>a</sup>
	HF/ STO-3G	MP4	HF/ 6-31G**	MP2	MP4	
$O_2 \rightarrow 2O$	0.70	3.94	1.36	5.16	4.70	(5.10)
$H_2O_2 \rightarrow HO^*$	0.96	2.47	0.01	2.39	2.14	(2.22)
$H_2O_2 \rightarrow H^* + HOO^*$	2.77	3.45	2.78	3.95	3.85	(3.78)
$H_2O \rightarrow H^* + HO^*$	3.66	4.43	3.73	5.15	5.04	(5.16)

<sup>a</sup> Reference 12.

further decrease of 0.2 eV could be included because of the zero-point vibrational energy of the O–H bond in  $H_3O^+$ . These contributions would yield an approximate proton solvation energy that underestimates experiment by about 0.1 eV. A full treatment of solvation would include the energetics for rearrangement of the three  $H_2O(l)$  molecules to form the  $H_3O^+$  solvation shell and further rearrangements for solvation of the  $H_3O^+(H_2O)_3$  complex. The present results imply that the energy for these rearrangements is less than a few tenths of an electronvolt.

**b. Bond Strengths.** The calculated bond strengths in Table 2 support the use of MP2/6-31G\*\* calculations for the oxygen reduction study; the HF/STO-3G and HF/6-31G\*\* seriously underestimate the O–O and O–H bond strengths. Adding MP4 to the former brings improved but still inadequate accuracy. The average MP2/6-31G\*\* error is 0.10 eV, smaller than the 0.17 eV average error for the MP4/6-31G\*\* bond strengths. Had zero-point vibrational energies been included, the average error for the former calculations would be very small. MP2 calculation times are shorter than those for MP4. Consequently both computational accuracy and speed favor the MP2 approach, which is why it has been chosen for the work that is presented below.

**c. Estimating  $U^\circ$ .** The relationship between energy for a reduction reaction and its reversible potential is

$$\Delta G^\circ = -nFU^\circ \quad (19)$$

where  $\Delta G^\circ$  is the change in Gibbs energy for the reaction,  $n$  is the number of electrons used in the reaction, and  $U^\circ$  is the reversible reduction potential. While it is in principle possible to calculate the enthalpic and entropic contributions which, when added to the calculated reaction energies, would convert them formally to Gibbs reaction energies, this is not done here. Instead

**Table 3.** Calculated Reaction Energies,  $E_r$  (eV), from the MP2/6-31G\*\* Method ( $\Delta G^\circ_{298}$  (eV) Incorporate Empirical Enthalpies of Heating and Third-Law Entropies into  $E_r$  As Explained in the Text; Reversible Electrochemical Potentials,  $U^\circ$  (V), from Eqs 20 and 25 Are Given in Parantheses)

reaction	$E_r$	$U^\circ$	$\Delta G^\circ_{298}$	$U^\circ$	(expt1) <sup>a</sup>
$O_2(g) + 2H^+(aq) + 2e^- \rightarrow H_2O_2(aq)$	-0.286	(0.14)	-1.064	(0.61)	(0.695)
$H_2O_2(aq) + H^+(aq) + e^- \rightarrow HO^\bullet(g) + H_2O(aq)$	-0.107	(0.11)	-0.691	(0.54)	(0.713)
$O_2(g) + 4H^+(aq) + 4e^- \rightarrow 2H_2O(aq)$	-2.891	(0.72)	-4.732 <sup>b</sup>	(1.18 <sup>b</sup> )	(1.229)
$H_2O_2(aq) + 2H^+(aq) + 2e^- \rightarrow 2H_2O(aq)$	-2.605	(1.30)	-3.570	(1.71)	(1.763)
$HO^\bullet(g) + H^+(aq) + e^- \rightarrow H_2O(aq)$	-2.498	(2.50)	-2.878	(2.88)	(2.813)

<sup>a</sup> Reference 12. <sup>b</sup>  $O_2$  zero-point energy term used for this reaction only.

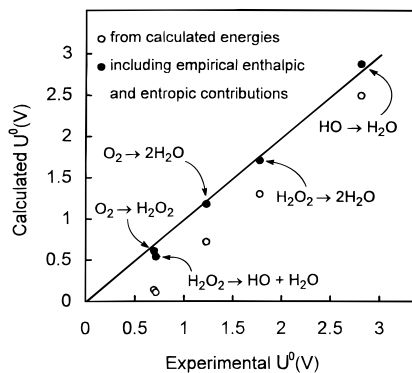


**Figure 1.** Calculated reversible potentials,  $U^\circ$  (V), vs experimental values based on reaction energies, circle, using eq 20 and free energies, dots, using eq 25 as discussed in section C.1.d.

available thermodynamic data are used. Table 3 contains  $U^\circ$  based on calculated gas-phase reaction energies,  $E_r$ , which are not corrected for zero-point energies, as calculated using the approximation used in ref 9,

$$U^\circ \approx \frac{-E_r}{nF} \quad (20)$$

along with approximate  $U^\circ$  values that are based on having added enthalpy changes for going from 0 to 298 K and zero-point and entropy contributions to  $E_r$  to yield  $\Delta G^\circ$ , and the experimental  $U^\circ$  values. Figure 1 shows the predicted values of  $U^\circ$  based both on the  $E_r$  and the approximate  $\Delta G^\circ$  values plotted as functions of the experimental values for reactions 6–8, 11, and 12. The  $U^\circ$  values derived from calculated reaction energies are, on average, 0.43 V lower than those based on the approximate  $\Delta G^\circ$  and the latter are very close to experiment, being on average 0.05 V low. It is proposed that half of the 0.43 eV discrepancy is due to omitting the hydrogen-bond annihilation energy and the remainder of it is due to omitting the correction terms.

**d. Sample Calculation of Enthalpy and Entropy Contributions.** For making comparisons with experimental  $U^\circ$  values it is first necessary to determine the standard states used for the reactants and products in reactions 6–12. For all but the two reductions where  $HOO^\bullet$  is a product or a reactant, comparison of  $U^\circ$  obtained from  $G_f^\circ_{298}$  values in ref 12 with  $U^\circ$  listed in ref 12 indicates that the standard state of  $H_2O$  is liquid, for  $H_2O_2$  it is 1 M (aq), and for  $HO^\bullet$  and  $O_2$  it is gas. Therefore, in adding  $T\Delta S$  and other terms to the calculated  $E_r$  values for obtaining approximate  $\Delta G^\circ$ , these standard states must be used. A sample calculation for the four-electron reduction to water proceeds as follows, where enthalpy contributions are for going from 0 K to the final state. Enthalpies, third-law entropies, and vaporization energies from ref 12 are

employed:

$$\begin{aligned} O_2[0K \rightarrow 298K(g)] & 0.08998 \text{ eV enthalpy contribution} - \\ & 0.6334 \text{ eV } T\Delta S \text{ contribution} + \\ & 0.0979 \text{ eV zero-point energy contribution} = -0.4455 \text{ eV} \quad (21) \end{aligned}$$

$$\begin{aligned} H_2O[0K \rightarrow 298K(g)] & 0.10265 \text{ eV enthalpy contribution} - \\ & 0.58297 \text{ eV } T\Delta S \text{ contribution} - (0.08904 \text{ eV})(\Delta G_f^\circ(l) - \\ & \Delta G_f^\circ(g)) \text{ contribution} = -0.5694 \text{ eV} \quad (22) \end{aligned}$$

$$\begin{aligned} H^+[0K \rightarrow 298K(aq)] & 0.065 \text{ eV } T\Delta S \text{ contribution}^{37} + \\ & 0.22812 \text{ eV hydrogen-bond annihilation contribution} = \\ & 0.2868 \text{ eV} \quad (23) \end{aligned}$$

Thus, for reaction 7, with the electron provided at  $U = 0$  V,

$$\begin{aligned} \Delta G^\circ \approx & -2.8912 \text{ eV (for } E_r) + 0.4455 \text{ eV (for } O_2) - \\ & 1.1472 \text{ eV (for } 4H^+) - 1.1387 \text{ eV (for } 2H_2O) = - \\ & 4.732 \text{ eV} \quad (24) \end{aligned}$$

and, for equilibrium, the electrons must be at potential  $U^\circ$ :

$$U^\circ = -\frac{\Delta G^\circ}{nF} = 1.18 \text{ V (1.229 V experimental)} \quad (25)$$

This and other similarly determined values are given in Table 3 and Figure 1. Reactant and product H–O bond vibrational zero-point energies are assumed to cancel in these determinations.

**2.  $O_2$  Reduction.** The four one-electron steps in reactions 9–12 have been studied by calculating the activation energies at potentials in the range of 0 to 2 V (SHE).  $H^+(aq)$  for these calculations was modeled by  $H_3O^+(H_2O)_2$ , wherein the hydronium ions had one  $H^+$  available for transfer to the species undergoing reduction. The fully optimized structure, which is the last entry in Table 1, was used. This 2-fold coordinated hydronium ion is almost 1 eV less stable than the 3-fold coordinated one: 1 eV is an upper limit for the rearrangement energy needed to achieve the reaction precursor configuration. However, the transferring proton could be stabilized some by adding one or two additional water molecules to the model. Adding these to the calculations would decrease the electron affinity of the reactants. Using a larger basis set would have an opposite influence by increasing the electron affinity. These influences and the effects of extending the solvation are worth further exploration, but the present model is tractable and establishes trends and provides understanding.

The species that are to be reduced ( $O_2$ ,  $HO_2^\bullet$ ,  $H_2O_2$ ,  $HO^\bullet$ ) interact with the solvated hydronium ion and form hydrogen-bonded complexes. These complexes were considered the precursors for the reduction reactions. The activation energies were calculated with respect to these minima.

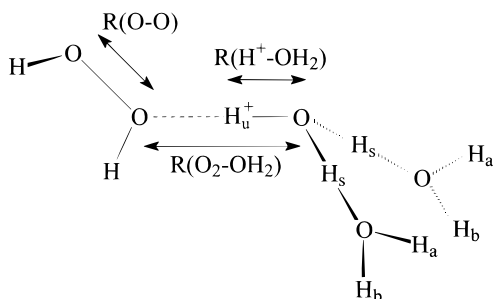


**Figure 2.** Definition of variables optimized in determining hydrogen-bonded precursor and transition state structures. The hydrogen peroxide molecule is shown for example. The bond angles were chosen as discussed in the text. The labels a, b, s, and u are used in Table 1.

**Table 4.** Calculated Equilibrium Internuclear Distances,  $R_e$  (Å), and Angles,  $\theta_e$  (deg), for  $O_2$ ,  $HOO^\bullet$ ,  $H_2O_2$ , and  $H_2O$  (MP2/6-31G\*\* Results Are Given; Experimental Results Are Given in Brackets)

molecule	$R_e(O-O)$	$R_e(HO)$	$\theta_e(HOO)$
$O_2^a$	1.247 [1.208]		
$HOO^\bullet^b$	1.326 [1.331]	0.975 [0.971]	104.43 [104.30]
$H_2O_2^{b,c}$	1.467 [1.464]	0.968 [0.965]	98.61 [99.40]
$HO^\bullet^a$		0.972 [0.970]	
$H_2O^{b,d}$		0.961 [0.957]	

<sup>a</sup> Experimental result from ref 33. <sup>b</sup> Experimental results from: *Landolt-Börnstein: Structure Data of Free Polyatomic Molecule*; Kuchitsa, K., Ed.; Springer: Berlin, 1995; Vol. XXIII. <sup>c</sup> The dihedral angle is 120.42° [111.80°]. <sup>d</sup> The HOH angle is 103.72° [104.51°].

The hydrogen-bonded precursor structures and energies were calculated with structure constraints to simplify the calculations. After initial structure optimization, the  $[-OH_2(OH_2)_2]$  structure was kept rigid and only three geometric variables were varied in precursor and transition state  $R-O\cdots H^+-OH_2(OH_2)_2$  structures. They were the  $R-O$  distance ( $R$  is  $O$ ,  $HO$ , or  $H$ ), the  $H^+-O$  distance, and the  $O-O$  distance, as shown in Figure 2. The  $O-H^+-O$  part was kept linear and the other bond distances, angles, and, when present, dihedral angles of the  $O_2$ ,  $HO_2^\bullet$ ,  $H_2O_2$ , and  $HO^\bullet$  reduction centers were fixed at the respective  $HO_2^\bullet$ ,  $H_2O_2$ ,  $HO^\bullet$ , and  $H_2O$  product values during the transition state determinations. In the case of  $H_2O_2$  reduction,  $H^+$  was kept in an  $HOO$  plane and  $H_2O_2$  angles were those of the dissociated products. For the precursor structure and energy determinations  $R-O$  angles were fixed at the reactant values while the  $R-O-H^+$  angles were fixed at the product values. Zero-point energies were not added to reactant, transition state, or product energies.

The activation energies were found by stepping through  $R_{O_2-OH_2}$  and  $R_{H-OH_2}$  in 0.01 Å increments and for each pair of points varying  $R_{O-O}$  (or  $R_{H-O}$  in the case of  $HO^\bullet$  reduction) until the reaction complex had the desired electron affinity. The energy to reach this structure was noted and the procedure was repeated to map out a locus of points of constant EA on the energy surface. The lowest energy on this locus yielded the activation energy and the corresponding structure was the transition state structure.

**a.  $O_2 + H^+ + e^- \rightarrow HOO^\bullet$ .** The calculated hydrogen bond strength between  $O_2$  and  $H^+-OH_2(OH_2)_2$  in this model was 0.047 eV. In the hydrogen-bonded complex the  $O-O$  distance decreased from the calculated gas-phase value of 1.247 Å [Table 4] to 1.217 Å. The hydrogen bond distance was 2.20 Å, and the  $H^+-O$  distance remained 0.97 Å. Hydrogen-bonded precursor parameters are given in Table 5.

**Table 5.** Calculated Key Internuclear Distances,  $R$  (Å), and Hydrogen Bond Strengths,  $E_{hb}$  (eV), for Hydrogen-Bonded Reduction Precursors (MP2/6-31G\*\* Results Are Given)

system	$R(H^+-O)$	$R(O\cdots H^+)$	$R(O-O)$	$E_{hb}$
$OO\cdots H^+-OH_2(OH_2)_2$	0.97	2.20	1.2172	0.047
$HOO\cdots H^+-OH_2(OH_2)_2$	0.98	1.83	1.3124	0.444
$HOHO\cdots H^+-OH_2(OH_2)_2$	0.98	1.76	1.4606	0.417
$HO\cdots H^+-OH_2(OH_2)_2$	0.99	1.76		0.565

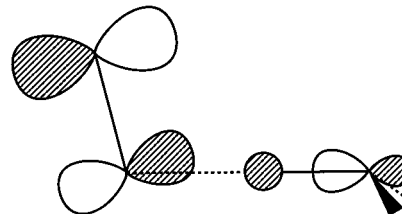


**Figure 3.** Orbital that accepts an electron at the transition state of first step in oxygen reduction.

The calculated activation energy for the first step is 0.924 eV at  $U = 0.727$  V. At this point the  $H^+-O$  bond is stretched by 0.12 to 1.09 Å, the  $OO$  bond is stretched by 0.0404 to 1.2576 Å, and the  $O_2-H^+$  distance is 1.35 Å. This is the most stable structure of the  $OO\cdots H^+\cdots OH_2(OH_2)_2$  complex with an electron affinity of 5.327 eV, which corresponds to the electrode potential of 0.727 V. Interestingly, the electron affinities of the two individual fragments but with the same structure parameters are 1.287 eV for  $H^+\cdots OH_2(OH_2)_2$  and  $-1.275$  eV for  $OO$ . Since these are several electronvolts less, and this would still be true even if additional diffuse functions were added to the basis set to increase the calculated value for  $O_2$  to the experimental value of 0.44 eV,<sup>38</sup> it might be concluded that the electric field of the hydronium ion enhances the electron affinity of  $OO$  or that orbital overlaps between  $OO$  and  $H^+$  enhance the electron affinity of  $H^+\cdots OH_2(OH_2)_2$ . The latter seems less likely to be a large effect because the  $H^+\cdots OO$  distance is long at 1.35 Å. Analysis of the orbitals shows that the solvated hydronium ion does indeed enhance the electron affinity of  $O_2$ . At the transition state structure, prior to the electron transfer, there are two empty  $\beta$ -spin  $O_2$   $\pi^*$ -based acceptor orbitals, one is pure  $\pi^*$  due to the plane of symmetry of the system and the other has a weak  $\sigma$  bonding overlap with the transferring proton (see Figure 3). These orbitals are quite stable at  $-2.84$  and  $-2.74$  eV, whereas for  $O_2$  with this bond length but with the hydronium ion absent they are much higher at 2.55 eV. This illustrates the effect of the electric field provided by the partially solvated proton on stabilizing  $O_2$   $\pi^*$  orbitals to enhance their electron affinity. After the electron transfers it occupies the in-plane  $\beta$ -spin-orbital, now at  $-6.96$  eV, and the other empty  $\beta$ -spin  $\pi^*$  orbital moves up to 7.82 eV. The half-filled  $\alpha$ -spin  $\pi^*$  orbitals also move up when the field of the proton is neutralized, from  $-19.82$  to  $-7.77$  eV for the in-plane one and from  $-20.98$  to  $-9.01$  eV for the other. Thus the  $OO$  becomes  $OO^-$  and the  $OO$  bond order is reduced from 2 to 3/2. Interestingly, while the net Mulliken  $OO$  charge went from 0.067 to  $-0.807$ , the net  $H_3O^+$  charge went from 0.783 to 0.699, a small decrease, indicating that at this stage  $H_3O^+$  and  $O_2^-$  are like an ion pair. Once this Born-Oppenheimer energy surface is entered, the energy drops rapidly as  $H^+$  leaves  $H_2O$  and bonds to  $O_2^-$ , forming  $HOO^\bullet$  with a 1.326 Å  $OO$  bond, which corresponds to its order of 3/2. Before the electron transfer, the departing  $H$  from  $H_3O^+$  bears a charge of 0.530 and the other two  $H$  are charged 0.525; after electron transfer their respective charges decrease slightly to 0.518 and 0.501.

**Table 6.** Calculated Key Transition State Internuclear Distances,  $R$  (Å), and Activation Energies,  $E_a$  (eV), at Various Potentials,  $U$  (V), for the Four Steps in  $O_2$  Reduction, Reactions 9–12 and  $H_2O$  Oxidation (MP2/6-31G\*\* Results Are Given)

reaction	$U$	$R(H^+-O)$	$R(O\cdots H^+)$	$R(O-O)$ [or $R(H-O)$ ]	reduction $E_a$	oxidation $E_a$
$O_2 \leftrightarrow HOO^*$ (9)	0.000	1.04	1.47	1.2407	0.496	0.905
	0.300	1.06	1.42	1.2482	0.662	0.771
	0.727	1.09	1.35	1.2576	0.924	0.606
	1.000	1.11	1.31	1.2641	1.105	0.514
	1.250	1.14	1.27	1.2656	1.277	0.436
	1.500	1.17	1.24	1.2698	1.455	0.364
	1.750	1.20	1.21	1.2741	1.637	0.296
	2.000	1.23	1.18	1.2789	1.824	0.233
	$HOO^* \leftrightarrow H_2O_2$ (10)	0.000	0.99	1.71	1.3342	0.068
0.300		1.00	1.62	1.3445	0.115	1.855
0.727		1.02	1.52	1.3613	0.226	1.539
1.000		1.04	1.46	1.3676	0.322	1.363
1.250		1.06	1.41	1.3725	0.426	1.217
1.500		1.08	1.37	1.3801	0.542	1.082
1.750		1.10	1.33	1.3867	0.667	0.957
2.000		1.12	1.30	1.3975	0.799	0.840
$H_2O_2 \leftrightarrow H_2O + HO^*$ (11)		0.000	1.08	1.35	1.7572	1.116
	0.300	1.10	1.32	1.7771	1.274	1.727
	0.727	1.13	1.27	1.8018	1.514	1.540
	1.000	1.15	1.25	1.8209	1.675	1.428
	1.250	1.16	1.23	1.8425	1.826	1.329
	1.500	1.18	1.21	1.8585	1.981	1.234
	1.750	1.21	1.19	1.8683	2.139	1.143
	2.000	1.23	1.17	1.8840	2.301	1.054
	$HO^* \leftrightarrow H_2O$ (12)	0.000	0.97	2.16	[0.9812]	0.000
0.300		0.97	1.98	[0.9878]	0.000	2.740
0.727		0.99	1.78	[0.9686]	0.002	2.278
1.000		1.00	1.66	[0.9818]	0.011	2.014
1.250		1.02	1.58	[0.9666]	0.047	1.799
1.500		1.03	1.49	[0.9788]	0.098	1.601
1.750		1.06	1.43	[0.9878]	0.172	1.425
2.000		1.08	1.37	[0.9775]	0.254	1.257

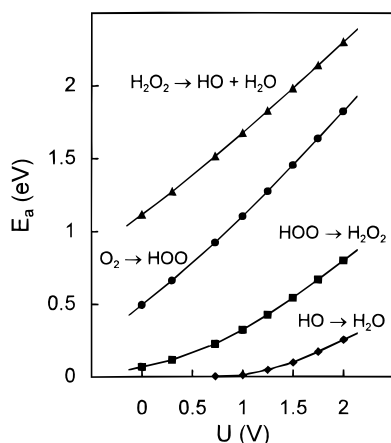
**Figure 4.** Calculated activation energies for the four one-electron oxygen reduction steps, eqs 9–12, as functions of electrode potential.

Table 6 contains the transition state structure parameters and activation energies found for all four reactions at the electrode potentials studied. Activation energies are graphed in Figure 4. The activation energies become smaller as the potential decreases and the reaction occurs sooner (smaller  $R(O-H^+)$  and  $R(O-O)$  and larger  $R(H^+\cdots O)$ ).

**b.  $HOO^* + H^+ + e^- \rightarrow H_2O_2$ .** As Figure 4 shows, the activation energy for the second reduction step, leading to  $H_2O_2$  formation, is much lower than that for the first step. The first step is concluded to be the slow one in uncatalyzed hydrogen peroxide formation.

When the  $H-O-O$  angle is set equal to that of  $H_2O_2$ , the  $O-O$  distance increases 0.011 Å, the  $H-O$  distance decreases 0.007 Å, and the energy increases 0.033 eV. Thus, the constraint of using the product angles for the transition state has a small

energetic cost. A hydrogen bond of 0.444 eV strength was calculated for the  $HOO\cdots H^+-OH_2(OH_2)_2$  interaction, and the  $O-O$  distance decreased 0.014 to 1.312 Å, the hydrogen bond distance was 1.83 Å, and the  $H^+-O$  bond distance increased by 0.013 to 0.98 Å. The largest difference between this hydrogen bond and the one involving  $O_2$  discussed previously is its order of magnitude greater strength and 0.37 Å shorter distance. The relatively greater strength is attributed to an electrostatic  $H^+$  monopole-OOH dipole attraction. The respective  $HOO^*$  atomic Mulliken charges are 0.380, -0.303, and -0.077. When  $HOO^*$  is hydrogen bonded to the hydronium ion, polarization changes the charges to 0.448, -0.261, and -0.121. That the greater strength is caused by the electrostatic interaction is demonstrated by replacing  $H^+-OH_2(OH_2)_2$  by  $H_2O$  and calculating a significantly weaker hydrogen bond strength of 0.075 eV for the same orientation. This weaker bond has a 0.40 Å longer internuclear distance.

The calculated activation energy for the second reduction step is 0.179 eV, at  $U = 0.727$  eV, 0.745 eV less than that calculated for the first step at this potential. At the transition state the  $H^+-O$  bond is stretched to 1.02 Å, which is 0.07 Å less than that for the first reduction. The  $O_2\cdots H^+$  distance is 1.52 Å, which is 0.17 Å greater than that for the first step, and the  $O-O$  bond, at 1.3613 Å, has increased 0.0489 Å over its value in the hydrogen-bonded complex. The electron affinity of this complex is 5.327 eV. Examining the fragments as before, the electron affinity of  $H^+\cdots OH_2(OH_2)_2$  is 0.847 eV, 0.440 eV less than that in the  $O_2$  reduction case because of the lessened  $H^+-O$  bond stretch. The  $HOO^*$  fragment's electron affinity, -0.557 eV, is 0.718 eV greater than that for the  $O_2$  fragment, but even if diffuse functions were used on  $HOO^*$ , giving a ~2.0 eV increase in its electron affinity as was seen above for  $HO^*$ , it is clear that the enhancement provided by the field of the

hydronium ion is required for electron transfer at this potential. At the transition state, before the electron transfers, the lowest unoccupied molecular orbital (LUMO) is predominantly p-type on the receiving oxygen and has a O–H<sup>+</sup>  $\sigma^*$  component overlapping in a stabilizing way with it. After the electron transfer this becomes the highest occupied doubly filled lone-pair orbital. Again the complex has the form of an ion pair with H<sub>3</sub>O<sup>+</sup> coordinated to a lone-pair orbital on HOO<sup>-</sup>. The energy drops rapidly as HOOH forms and the O–O bond stretches to 1.467 Å, a single bond.

**c. HOOH + H<sup>+</sup> + e<sup>-</sup> → HO• + H<sub>2</sub>O.** A strong hydrogen bond forms between a HOOH oxygen lone-pair and the hydronium ion. As may be seen in Table 5, the O•••H<sup>+</sup> distance is about 1.76 Å and the strength is 0.417 eV. This strength is attributed to the electrostatic component of the bonding due to the -0.375 charge on each O. With hydrogen bonding the O charges become -0.478 and -0.282 due to polarization.

The calculated activation energy at the potential 0.727 V is the highest of all, 1.513 eV. At this point the H<sup>+</sup>•••O and O–O distances are both long, 1.13 and 1.8018 Å, respectively, and the O•••H<sup>+</sup> distance is short at 1.27 Å. In this case the transition state is further along the way to product structure than was the case for the previous two steps. Looking at the isolated fragments when given the transition state structures, the electron affinity is 1.604 eV for H<sup>+</sup>•••OH<sub>2</sub>(OH<sub>2</sub>)<sub>2</sub> and -0.750 eV for HOOH. As in the previous cases, the field of the hydronium ion is required for electron transfer at this voltage. The hydronium ion has a relatively high electron affinity in this case, due to the longer H<sup>+</sup>–O bond stretch, but it is still more than 3.0 eV less than that of the transition state complex, for which EA is 5.327 eV.

Prior to electron transfer at the transition state the LUMO is at -3.681 eV, having antibonding O•••H<sup>+</sup> and OO  $\sigma^*$  character. After electron transfer it becomes the half-filled HOMO at -7.849 eV and evolves into the HO radical orbital as the products separate.

**d. HO• + H<sup>+</sup> + e<sup>-</sup> → H<sub>2</sub>O.** In this case the hydrogen bond strength between HO• and H<sup>+</sup>–OH<sub>2</sub>(OH<sub>2</sub>)<sub>2</sub> was calculated to be 0.564 eV, 0.13 eV greater than that for the two previous results. The oxygen charge in the hydroxyl radical is -0.354, which changes to -0.340 in the hydrogen-bonded complex. The transition state comes very early when the potential is at 0.727 V, with the O•••H<sup>+</sup> distance at 1.78 Å, which is 0.02 Å longer than in the hydrogen-bonded complex, and the activation barrier is essentially zero. The electron affinity of the hydronium ion fragment is 0.735 eV and that of HO• is -0.164 eV, so once again, the field of the hydronium ion is what activates the electron transfer. At lower potentials the electron transfers as the reactants approach each other before the hydrogen-bonded precursor has a chance to form. As Figure 4 shows, this is the easiest of the four steps.

Before electron transfer, the lowest unoccupied  $\beta$ -spin-orbital lies at -1.296 eV and has p character on the receiving O. After electron transfer it becomes doubly occupied and lies at -6.873 eV. The net Mulliken charge on OH before electron transfer is 0.056 and after it is -0.796. Thus once again the system has the form of a partially charged ion pair, in which the proton will move with rapid stabilization down the new energy surface to form the product, an H<sub>2</sub>O molecule in this case.

**3. Summary of O<sub>2</sub> Reduction Results.** Selected energies along the four-electron reduction path are summarized in Figure 5. Here energies are plotted for the four reduction steps of O<sub>2</sub> to 2 H<sub>2</sub>O at potentials from 0.0 to 2.0 V. The increase in activation barriers with increase in potential is clear. Interest-

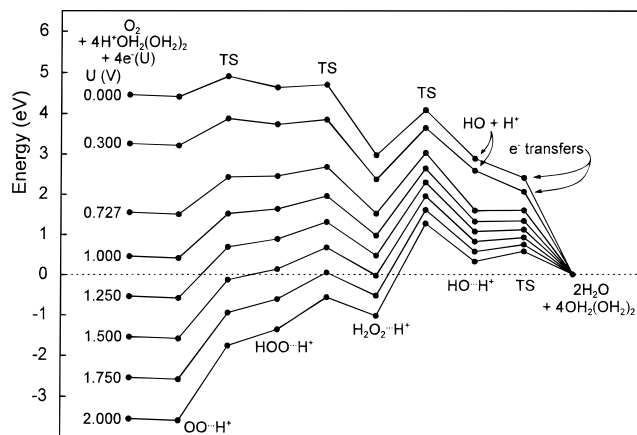


**Figure 5.** Energies as functions of electrode potential for the reaction system from beginning to end of the O<sub>2</sub> reduction sequence. Transition state (TS) and hydrogen bonded precursor (O•••H<sup>+</sup>) points are shown.

ingly, one can read an accurate  $U^{\circ}$  value for the four-electron process off of this figure. This coincidental result occurs because the solvated hydronium ion is destabilized by 1.0 eV by the removal of one H<sub>2</sub>O molecule and the solvated water product of each step is 0.56 eV destabilized with respect to three isolated H<sub>2</sub>O molecules. The net effect is that  $E_r$  for each one-electron step is decreased by 0.44 eV and, when used in eq 20, the predicted  $U^{\circ}$  are increased by 0.44 V, placing them almost in coincidence with the  $U^{\circ}$  values that were calculated based on the approximate  $\Delta G^{\circ}$  values. Using this graph, the predicted reversible potential, for the four-electron reduction of O<sub>2</sub> to water, is 1.18 V. This matches the value from Table 3. Figure 5 also shows how at potentials less than the four-electron process reversible potential (1.229 V) the reaction is downhill and that H<sub>2</sub>O<sub>2</sub> may be a trap at very low potentials.

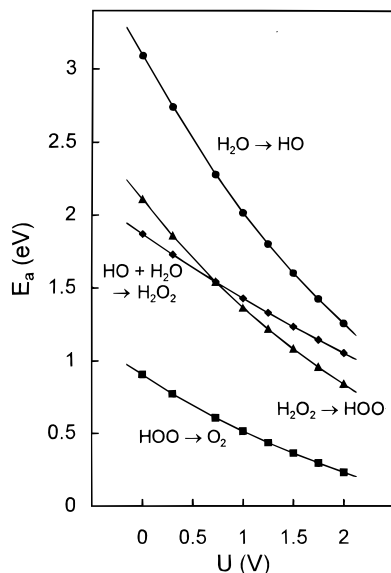
**4. Implications Regarding Catalyzed O<sub>2</sub> Reduction. a. Structure Effects.** From the above, it is evident that an efficient four-electron reduction catalyst must not liberate hydrogen peroxide and it must activate the first and third reduction steps without deactivating the other two steps. The kinetic difficulty for the third step, the hydrogen peroxide reduction, stems from the need to stretch the HO–OH bond by  $\sim 0.3$  Å to give it the needed electron affinity even in the presence of the very close hydronium ion. An electrode surface that stretches the HO–OH bond will increase the electron affinity because the OO  $\sigma^*$  acceptor orbital is stabilized when the HO–OH distance is increased. Complete dissociation on the electrode surface should lead to good activity, based on the low activation energy calculated for HO• reduction.

The first step of dioxygen reduction should be chemisorption-induced O–O bond lengthening too, for this enhances the electron affinity of the  $\pi^*$  acceptor orbitals. In basic electrolytes O<sub>2</sub><sup>-</sup>(ads) is thought to form,<sup>14</sup> but relatively negative potentials are required. In acid solution HOO(ads) should form at more positive potentials since a moderately strong adsorption bond will form stabilizing it. This bonding may have the effect of lowering the activation energy too.

**b. Electronic Effects.** As discussed in the previous section, bonding to the surface active site can enhance the electron affinity and activate the reduction of the O<sub>2</sub> or subsequent HOOH intermediate by causing the O–O bond to lengthen. It is in principle possible for the active site to further enhance the activity by increasing the electron affinity of the adsorbate plus surface reduction center beyond that caused by perturbing the structure of the oxygen species. Surfaces that stabilize the adsorbed reduction products through strong bonding are likely

**Table 7.** Calculated Key Internuclear Distances,  $R$  (Å), and Hydrogen Bond Strengths,  $E_{\text{hb}}$  (eV) for Hydrogen-Bonded Oxidation Precursors (MP2/6-31G\*\* Results Are Given)

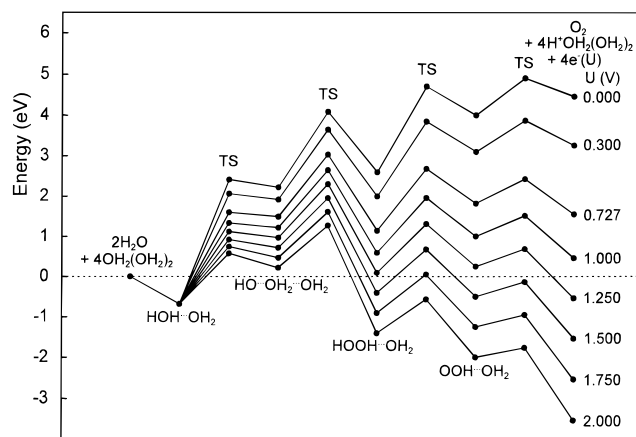
system	$R(\text{H}\cdots\text{O})$	$R(\text{O}-\text{H})$	$R(\text{O}-\text{O})$	$E_{\text{hb}}$
$\text{OO}-\text{H}\cdots\text{OH}_2(\text{OH}_2)_2$	1.50	1.03	1.3190	1.077
$\text{HOO}-\text{H}\cdots\text{OH}_2(\text{OH}_2)_2$	1.62	1.00	1.4700	0.794
$\text{HOHO}-\text{H}\cdots\text{OH}_2(\text{OH}_2)_2$	1.73	0.99	2.7779	0.671
$\text{HO}-\text{H}\cdots\text{OH}_2(\text{OH}_2)_2$	1.73	0.98		0.678

**Figure 6.** Calculated activation energies for the four one-electron water oxidation steps, eqs 12–9, as functions of electrode potential.

to do this, as will be shown in an upcoming paper concerning a platinum electrocatalyst.<sup>39</sup>

**5. H<sub>2</sub>O Oxidation.** It is possible to calculate, within the same model, reaction energies and activation energies for the oxidation of H<sub>2</sub>O to O<sub>2</sub> by the sequence of reactions beginning with eq 12 and ending with eq 9. Proceeding in the reverse direction, each reaction has loss of an electron and a proton. The transition states are the same as for the reduction steps, and the hydrogen-bonded precursors have the OH<sub>2</sub>(OH<sub>2</sub>)<sub>2</sub> units in the hydronium ion structure as used above. The precursor structures are given in Table 7 and the angles are the same as were used for reduction precursors and transition states.

Calculated activation energies for the four steps of H<sub>2</sub>O oxidation are included in Table 6 and graphed in Figure 6. All increase as the electrode potential increases. The highest is for the first step, generating OH from H<sub>2</sub>O by electron and proton

**Figure 7.** Energies as functions of electrode potential for the reaction system from beginning to end of the H<sub>2</sub>O oxidation sequence. Transition state (TS) and hydrogen bonded precursor (O...H) points are shown.

loss. This is 1.7 eV at the reversible potential, and at this potential HO• oxidation is next with 1.3 eV followed by H<sub>2</sub>O<sub>2</sub> with 1.2 eV and the last step, HOO• reduction, has the smallest calculated activation energy, 0.4 eV.

A summarizing graph, Figure 7, shows that at all of the potentials considered the reaction is uphill though the second transition state and H<sub>2</sub>O<sub>2</sub> is a trap. Catalyzing the oxidation of water will be addressed in ref 39.

#### D. Summary

A methodology has been systematically applied to calculating transition state structures and activation energies for outer-sphere oxygen reduction and water oxidation over the 0–2 V electrode potential range. The results are reasonable, yielding a high barrier for the first step in H<sub>2</sub>O<sub>2</sub> reduction. The approach could be applied to other reactions and to catalysis of these<sup>39</sup> or other reactions. Explorations into enhancing the model to a larger reaction complex with (i) one or two additional H<sub>2</sub>O molecules coordinated to the transferring proton, (ii) interaction with solvated counterions, (iii) solvation of the reaction complex, and (iv) exploring larger basis set effects are logical extensions. For establishing trends and getting relative activation energies for a series of reaction steps and for understanding the influence of a third body, a catalyst, the model as applied above may be sufficient.

**Acknowledgment.** T.V.A. is grateful to the Case Western Reserve University Chemistry Department for support. This work is also partially supported by a grant from the U.S. Army Research Office, No. DAAD 19-99-1-0253.

(39) Anderson, A. B.; Albu, T. V. Manuscript in preparation.